Received: 27 November 2023 | Accepted: 12 July 2024

DOI: 10.1111/iej.14126

INTERNATIONAL ENDODONTIC JOURNAL | WILEY

ORIGINAL ARTICLE

Proanthocyanidin surface preconditioning of dental pulp stem cell spheroids enhances dimensional stability and biomineralization in vitro

Shengyan Yang[1] | **Andy Yu Pan Leung**[1] | **Zheng Wang**[2] | **Cynthia Kar Yung Yiu**[3] | **Waruna Lakmal Dissanayaka**[1]

[1]Applied Oral Sciences & Community Dental Care, Faculty of Dentistry, The University of Hong Kong, Hong Kong SAR, China

[2]Department of Mechanical Engineering, The University of Hong Kong, Hong Kong SAR, China

[3]Paediatric Dentistry & Orthodontics, Faculty of Dentistry, The University of Hong Kong, Hong Kong SAR, China

Correspondence
Waruna Lakmal Dissanayaka, Applied Oral Sciences & Community Dental Care, Faculty of Dentistry, The University of Hong Kong, Hong Kong SAR, China.
Email: warunad@hku.hk

Abstract

Aim: Lack of adequate mechanical strength and progressive shrinkage over time remain challenges in scaffold-free microtissue-based dental pulp regeneration. Surface collagen cross-linking holds the promise to enhance the mechanical stability of microtissue constructs and trigger biological regulations. In this study, we proposed a novel strategy for surface preconditioning microtissues using a natural collagen cross-linker, proanthocyanidin (PA). We evaluated its effects on cell viability, tissue integrity, and biomineralization of dental pulp stem cell (DPSCs)-derived 3D cell spheroids.

Methodology: Microtissue and macrotissue spheroids were fabricated from DPSCs and incubated with PA solution for surface collagen cross-linking. Microtissue viability was examined by live/dead staining and 3-(4,5-dimethylthiazol-2-yl)−2,5-diphenyltetrazolium bromide (MTT) assay, with transverse dimension change monitored. Microtissue surface stiffness was measured by an atomic force microscope (AFM). PA-preconditioned microtissues and macrotissues were cultured under basal or osteogenic conditions. Immunofluorescence staining of PA-preconditioned microtissues was performed to detect dentin sialophosphoprotein (DSPP) and F-actin expressions. PA-preconditioned macrotissues were subjected to histological analysis, including haematoxylin–eosin (HE), alizarin red, and Masson trichrome staining. Immunohistochemistry staining was used to detect alkaline phosphatase (ALP) and dentin matrix acidic phosphoprotein 1 (DMP-1) expressions.

Results: PA preconditioning had no adverse effects on microtissue spheroid viability and increased surface stiffness. It reduced dimensional shrinkage for over 7 days in microtissues and induced a larger transverse-section area in the macrotissue. PA preconditioning enhanced collagen formation, mineralized nodule formation, and elevated ALP and DMP-1 expressions in macrotissues. Additionally, PA preconditioning induced higher F-actin and DSPP expression in microtissues, while inhibition of F-actin activity by cytochalasin B attenuated PA-induced dimensional change and DSPP upregulation.

Conclusion: PA surface preconditioning of DPSCs spheroids demonstrates excellent biocompatibility while effectively enhancing tissue structure stability and promoting biomineralization. This strategy strengthens tissue integrity in DPSC-derived spheroids and amplifies osteogenic differentiation potential, advancing scaffold-free tissue engineering applications in regenerative dentistry.

KEYWORDS

cell spheroids, collagen cross-linking, dental pulp stem cells, proanthocyanidin, scaffold-free tissue engineering

INTRODUCTION

Pulp regeneration has been at the forefront of regenerative dentistry in recent years, with numerous biomedical approaches mainly categorized as scaffold-based or scaffold-free strategies (Dissanayaka & Zhang, 2020). The scaffold-free approach involves prefabricated multicellular units in spheroids, cell sheets, and tissue strands (Dissanayaka & Zhang, 2020; Ovsianikov et al., 2018). These cellular constructs secrete a favourable extracellular matrix (ECM) and self-assembly to fuse into large cohesive tissues, permitting dynamic cellular interactions between and among host and transplanted cells without a mediator material (Dissanayaka & Zhang, 2020; Kelm et al., 2006; Kelm & Fussenegger, 2004). Our previous study demonstrated that human umbilical vein endothelial cell (HUVEC)-incorporated scaffold-free microtissue spheroids of human dental pulp stem cells (DPSCs), when transplanted in vivo, can give rise to vascularized dental-pulp-like tissue (Dissanayaka et al., 2014). However, compared to scaffold-based methods, tissue construct lacks adequate mechanical strength, tends to distort or wash away during manipulation, and could shrink over time (Shearier et al., 2016, Schmal et al., 2016, Redondo-Castro et al., 2018, Deynoux et al., 2020, Bellotti et al., 2016). Hence, there is an imminent need for effective strategies to ensure the structural integrity of microtissue spheroids.

Collagen, a major ECM protein, serves critical functions within cell spheroids, including initiating spheroids formation, maintaining spheroid structure, favouring cell viability, and stem cell lineage-specific differentiation (Calori et al., 2022; Gonzalez-Fernandez et al., 2022; Gu et al., 2019; Kim et al., 2021; Shajib et al., 2022; Sorushanova et al., 2019). Recent studies have explored the use of collagen-based biomaterials to encapsulate cell spheroids, yielding positive outcomes for biomedical applications (He et al., 2021; Kageyama et al., 2023; Li et al., 2021); nevertheless, it adds additional steps during the application procedure. Collagen cross-linking is a significant additional modification of collagen fibres (Adamiak & Sionkowska, 2020), which prevents collagen molecules from sliding past each other under stress, enhancing its overall mechanical stability and minimizing collagen degradation (Gu et al., 2019; Sorushanova et al., 2019). Collagen cross-linking can be achieved through various exogenous methods, including chemical, physical and biological approaches (Adamiak & Sionkowska, 2020; Gu et al., 2019; Sorushanova et al., 2019), endowing its wide-range applications in medicine and tissue engineering, including skin wounds repair, tendon and cartilage repair, treatment of corneal and cardiovascular diseases, bone and neural tissue engineering (Gu et al., 2019, Sorushanova et al., 2019). Given its significance in enhancing tissue mechanical stability, we expect to facilitate collagen cross-linking in cell spheroids surface of ECM by simply preconditioning with collagen cross-linker, reducing the degradation or shrinkage of tissue constructs.

Chemical collagen cross-linkers have been widely utilized in scaffold-based tissue engineering, such as glutaraldehyde (GA), genepin, formaldehyde, chitosan, and proanthocyanidin (PA) (Walters & Stegemann, 2014; Zheng et al., 2023). With antioxidative, antimicrobial, and anti-inflammatory properties (Chen et al., 2022; Rauf et al., 2019), PA, the plant-derived phenolic polymer, has been employed as a natural cross-linking agent for collagen matrices in scaffold-based approaches and has shown various benefits (Han et al., 2003). When porous gelatin scaffolds were cross-linked with PA and GA, it was shown that PA-cross-linked scaffolds were non-cytotoxic and promoted the attachment and proliferation of the seeded cells. In contrast, fewer cells were seen on GA cross-linked scaffolds (Yang et al., 2017). In addition, the use of collagen/oligomeric proanthocyanidin/oxidized hyaluronic acid composite scaffolds in the regeneration of articular cartilage showed high biocompatibility and excellent mechanical properties, and in vivo testing revealed signs of angiogenesis and new bone formation (Lee et al., 2021).

Furthermore, a barrier membrane made from type-I collagen and cross-linked by oligomeric proanthocyanidins demonstrated cell proliferation faster on the PA-treated collagen film than in the cell culture flask. It

promoted osteoblast differentiation, producing higher alkaline phosphatase (ALP) activity and mineralization (Yang et al., 2021). However, the use of PA in a scaffold-free approach as a preconditioning agent has not been studied, and it is a novel approach.

In light of the challenges faced by scaffold-free approaches and the potential benefits of collagen cross-linking, we propose surface preconditioning of DPSCs-fabricated microtissue spheroids with collagen cross-linkers to create a surface layer consisting of cross-linked collagen from ECM. We hope that the surface treatment with collagen cross-linkers could enhance the structural integrity of tissue spheroids and promote biological mechanisms such as cell proliferation and osteogenesis. We aimed to assess how the surface cross-linking of the microtissue spheroids by PA affects cell viability, structural stability, and mineralized tissue formation.

MATERIALS AND METHODS

The manuscript of this laboratory study has been written according to Preferred Reporting Items for Laboratory Studies in Endodontology (PRILE) 2021 guidelines (Figure 1).

Cell and tissue culture

Human dental pulp stem cells (DPSCs) were purchased from Lonza (Basel, Switzerland). Our previous study confirmed and reported the cells' mesenchymal origin and multipotent differentiation ability (Zhang et al., 2021). DPSCs from passage 2 were used for fabricating 3D microtissues and, after that, macrotissue spheroids. DPSCs, microtissue, and macrotissue spheroids were all incubated at 37°C 5% CO_2 humid atmosphere, and cultured in basal culture medium: minimal essential medium alpha medium (α-MEM, Gibco, USA) supplemented with 15% fetal bovine serum (FBS, Gibco, A5256701, UK), 100 units/mL penicillin and streptomycin (Gibco,15 140–122). The culture medium was changed every 2–3 days.

Fabrication of 3D DPSCs microtissue and macrotissue spheroids

DPSCs microtissue spheroids were fabricated using agarose 3D petri dishes made with 12-series micro-moulds (MicroTissues, Inc., Sharon, MA, USA). As reported previously (Dissanayaka et al., 2015), 500 μL of 2% molten agarose (BIOWEST AGAROSE, BY-R0100, Spain) was pipetted into the mould that contains 256 microwells under aseptic conditions. Once agarose gelled, micro-moulds were carefully flexed to separate the 3D Petri dish. Before DPSC single cell suspension was seeded into a 3D Petri dish, the dish was equilibrated with cell culture medium for 30 mins. The cell number of seeded DPSCs was calculated to ensure an equal amount of DPSCs (86×10^4/190 μL) was seeded into each 3D Petri dish. After seeding the cells, Petri dishes were kept static for 10 min to ensure cells settled evenly into each microwell, and then cell culture medium was gently added. After incubating at 37°C in a 5% CO_2 atmosphere for 2 days, seeded DPSCs aggregated and self-assembled into microtissue spheroids as demonstrated in Figure 2; the microtissue spheroids were harvested from the Petri dishes and used for the following assays.

For fabricating each macrotissue spheroid, well-assembled microtissues from one Petri dish (approximately 768 microtissues) were transferred to a custom-designed, 3 mm-diameter, agarose cylindrical mould as previously reported (Dissanayaka et al., 2015). These microtissues were cultivated in 12-well plates for 4 days to allow them to self-assemble and amalgamate into macrotissues, then used for the subsequent assays.

Proanthocyanidin (PA) treatment

Purified grape seed oligomeric proanthocyanidins (PA) were purchased from United States Pharmacopoeia (USP, Catalogue No: 1298219). Different concentrations of PA solution (1, 2, and 4 mg/mL) were added to cultured DPSCs for 1, 10, 30, and 60 min, respectively. For microtissue spheroids, 1 mg/mL PA solution was added for 1, 10, 30, and 60 min, respectively. 0.01% glutaraldehyde (GA, Electron Microscopy Sciences) treatment for 1 min was used as the positive control, and the same volume of culture medium was used as the negative control. For macrotissue spheroids, 1 mg/mL PA solution was added for 30 or 60 min, and culture medium was utilized as the negative control group. PA-treated and control macrotissue spheroids were cultured in basal or osteo−/odontogenic (OS) induction medium: α-MEM medium supplemented with 5% FBS, 100 units/mL penicillin, and streptomycin, 10 mM β-glycerophosphate (Sigma-Aldrich, 50 020-100G, USA), 0.2 mM L-ascorbic acid (Sigma-Aldrich, A5960-25G, USA), and 0.1 mM dexamethasone (Sigma-Aldrich, D1756-25MG, USA), for 7 days or 14 days, respectively. To disrupt the polymerization of cytoskeletal actin, the cell-permeable mycotoxin cytochalasin B (CB, Santa Cruz Biotech, CAS 14930–96-2, 2 μM) was used to treat microtissues together with PA for 60 min.

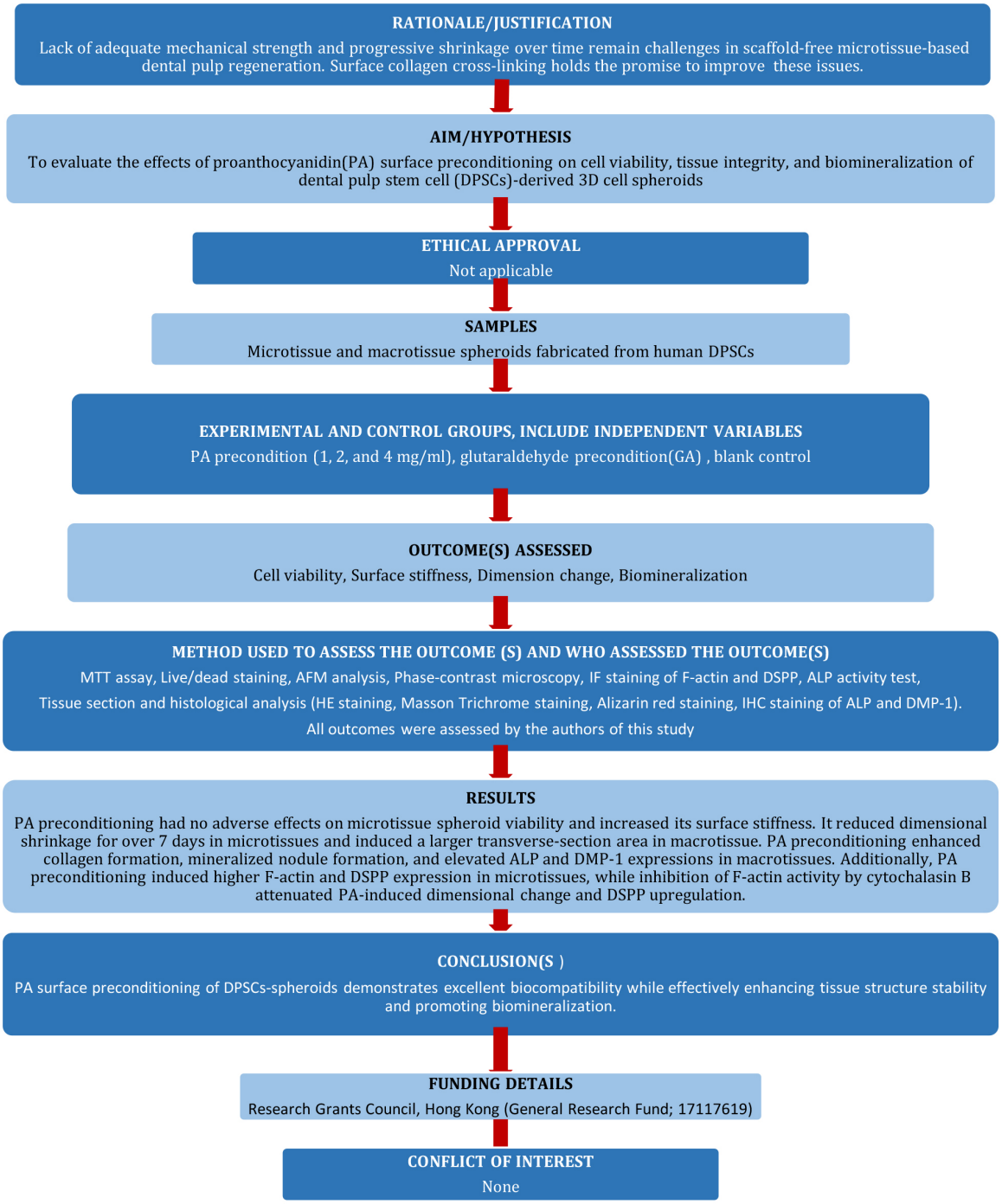

FIGURE 1 PRILE 2021 flowchart.

MTT and live/dead assay

After being treated with PA solution (1, 2, 4 mg/mL) for specific time durations (1, 10, 30, 60 min) or treated with 0.01% GA solution or culture medium, cell viability of DPSCs was assessed by 3-(4,5-dimethylthiazol2-yl)-2,5-di phenyltetrazolium bromide (MTT, Sigma-Aldrich, USA) assay, the absorbance OD value of each well was measured at 570 nm. Ten independent duplicates were conducted for each group.

For live/dead assay, microtissue spheroids were treated with 1 mg/mL PA solution for 10, 30, and 60 min. 0.01% GA treatment for 1 min was used as the positive control, and culture medium was used as the negative control. Treated microtissue spheroids were incubated with acridine orange (AO) and propidium iodide (PI) in a 1:1 ratio for 30 mins. Images of each microtissue spheroid were recorded under a confocal laser scanning microscope on Day 0 (immediately after treatment), Day 1, Day 3, and Day 7. Dead cell numbers in each microtissue spheroid

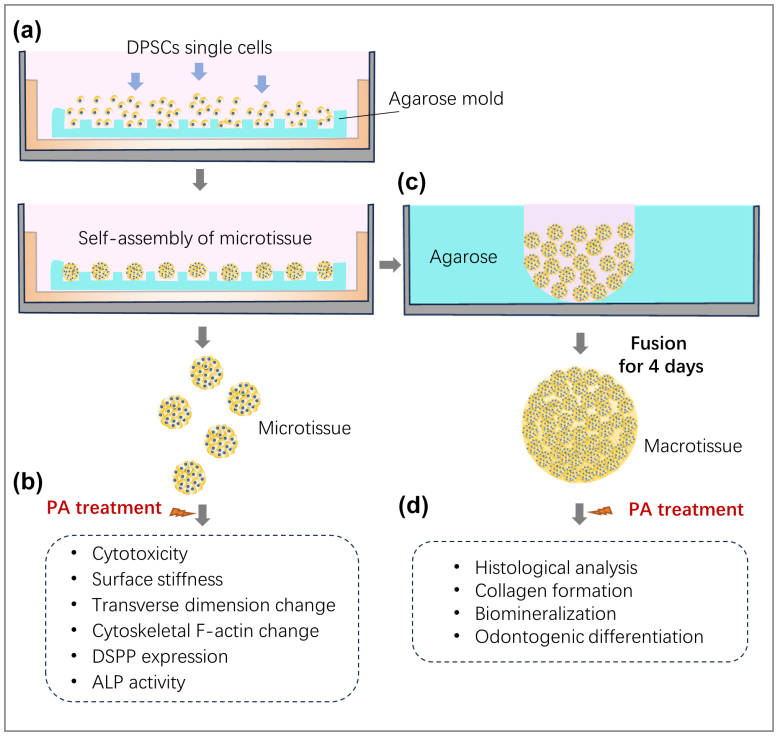

FIGURE 2 Schematic diagram of the experimental procedure. (a) DPSC cell suspensions were seeded into the agarose mould. After 2 days, DPSCs self-assembled into microtissue spheroids. (b) Fabricated microtissue spheroids were used to assess the effect of PA treatment on cytotoxicity, surface stiffness change, dimensional change, cytoskeletal F-Actin, DSPP expression and ALP activity change. (c) Well-assembled microtissues were collected for fusing into macrotissues. (d) After placing the patient in agarose mould for 4 days, PA treatment was performed, and the patient was cultured under basal or OS culture medium for 7 or 14 days. Histological and immunohistochemical analysis was performed to evaluate the tissue structure integrity, collagen formation, biomineralization and odontogenic differentiation of the PA-treated macrotissues.

were counted using ImageJ software. Three independent duplicates of each group were conducted for live/dead assay (each group $n = 3$).

Surface stiffness measurement

Surface stiffness of microtissue spheroids was measured using the atomic force microscope (AFM) (JPK NanoWizardII, Bruker) in combination with a tipless silicon cantilever (Cat No.: TL-CONT-20), which is $2.0 \pm 1\,\mu m$ thick, $450 \pm 10\,\mu m$ long, and $50 \pm 7.5\,\mu m$ wide. Force curves were taken in fluid (water) for each microtissue spheroid with the spring of 0.335 N/m under contact mode, then fitted to the Hertz model for calculating stiffness value (each group $n = 9$).

Immunofluorescence (IF) staining

Microtissues were fixed with 4% PFA, then blocked with 5% bovine serum albumin (BSA, Beyotime Institute of Biotechnology, China), after that, incubated with DSPP antibody (Santa Cruz, sc-73 632, 1:50), secondary antibody Anti-mouse IgG (H + L), F(ab')2 Fragment (Alexa Fluor® 488 Conjugate) (CST, #4408, 1:300) and Actin-Tracker Green-488 (Beyotime, Shanghai, China; 1:200) for visualizing F-actin and 4′,6-diamidino-2-phenylindole (DAPI) for cell nucleus. Microtissues were observed under a confocal laser scanning microscope (Zeiss LSM 900, Carl Zeiss, Germany). IF intensity of F-actin (each group $n = 10$) and DSPP (each group $n = 6$) were quantified using the ImageJ software.

Spheroids area measurement

After treating with 1 mg/mL PA solution for 60 min, images of microtissue spheroids were taken using phase-contrast microscopy (Nikon, Tokyo, Japan) every 48 h until day 7. Microtissue spheroids with no treatment were used as a negative control. The transverse area of each microtissue spheroid was measured with the ImageJ software (each group $n = 23$). Microtissue spheroid dimensional change (%) was calculated by dividing the dimensions by those measured at day 0.

Haematoxylin–Eosin (HE), Masson trichrome & Alizarin red staining

Macrotissues treated with 1 mg/mL PA solution for 30 and 60 min or with culture medium were cultured in basal or OS medium for 7 days or 14 days. Macrotissues were then fixed with 4% paraformaldehyde (PFA) overnight, dehydrated through a gradient alcohol series, and embedded in paraffin blocks. Embedded microtissues were trimmed as 5 μm thick sections, next, dewaxed through 2 changes of xylene for 10 mins each, hydrated in 2 changes of 100% ethanol for 3 mins each, 95% and 70% ethanol for 1 min each, then rinsed in distilled water for 3 mins.

For haematoxylin–eosin (HE) staining, hydrated slides were stained with haematoxylin for 3 min, then washed with 0.1% acid alcohol for 3 s, and subsequently eosin for 1 min. For Alizarin red staining, sections were stained with 2% Alizarin red solution for 30 s. Masson's trichrome staining of hydrated slides was performed according to the manufacturer's protocol (Servicebio, Wuhan, China, G1006-20ML).

Images were captured under a bright field of the polarized microscope. The transverse tissue area of HE-stained slides was quantified by ImageJ software. For quantitative analysis of Masson's trichrome staining, the blue-stained collagen fibre area was quantified using the software ImageJ and divided by total tissue area to calculate the collagen area proportion. Quantitative analysis of Alizarin red staining was carried out by quantifying the red mineralized area using ImageJ software and dividing by the total tissue area to calculate the relative mineralized area. The mineralized nodule number of each macrotissue was also counted. At least triple duplicates were performed for each group.

Immunochemistry (IHC) staining

Immunohistochemistry staining of macrotissue sections was performed using Abcam Mouse and rabbit-specific HRP/DAB (ABC) Detection IHC kit (Abcam, #AB64264). According to the manufacturer's instruction, tissue slides underwent water-bath heating for antigen retrieval using the Dako Target Retrieval Solution, then incubated with primary antibodies: ALP (Abcam, ab65834, 1:100) and DMP-1 (Novus Biologicals, NBP1-89484, 1:100). Tissues without added primary antibody were used as an isotype control. Protein expression signals were visualized by DAB staining for 40 s. Images were captured using the inverted microscope. ALP and DMP-1 expression were quantified by measuring brown-stained areas using the ImageJ software. Protein-positive area proportion was calculated by dividing the overall area of the macrotissue under 5× microscope. At least triple duplicates were performed for each group.

Alkaline phosphatase (ALP) activity measurement

Microtissue spheroids treated with 1 mg/mL PA solution for 30 or 60 min were cultured for 14 days in either basal or OS medium. ALP activity of each microtissue spheroid was measured using an ALP Assay Kit (Colorimetric, Abcam, ab83369). Briefly, the microtissue spheroids were homogenized with ALP Assay buffer; then, the supernatant was collected and mixed with reaction substrates and p-nitrophenol. After incubation at 37°C for 30 min, its absorbance was measured at 405 nm. The protein concentration of microtissue spheroid was determined using the BCA protein assay kit (Thermo Fisher Scientific Inc., Waltham, MA), and ALP activity was then calibrated with the detected protein concentration (each group $n = 3$).

Statistic analysis

All data were presented as mean ± standard deviation (SD). Multiple group comparisons were analysed using the one-way analysis of variance (normal distribution and homogeneity of variance) or the Kruskal-Wallis *H*-test (nonnormal distribution or heterogeneity of variance). Fisher's least significant difference test was used for post hoc analysis. Statistical analyses were conducted using the GraphPad Prism 8 software (GraphPad Software, Inc., San Diego, CA). A *p*-value of $p < 0.05$ was considered statistically significant.

RESULTS

Effects of PA treatment on cell viability of microtissue spheroids

MTT assay in Figure 3a showed that 1 mg/mL and 2 mg/mL PA treatment for 1, 10, 30, and 60 min had no adverse effects on cell viability of DPSCs ($p > 0.05$). Compared with the blank control group, 4 mg/mL PA treatment for 30 mins showed reduced cell viability ($p < 0.05$). 0.01% GA treatment for 1, 10, 30, and 60 min significantly decreased DPSCs' cell viability ($p < 0.0001$). These results indicated that 1 and 2 mg/mL PA treatment cause no adverse effects on cell viability, 4 mg/mL treatment may cause potential effects on cell viability, and 0.01% GA treatment robustly

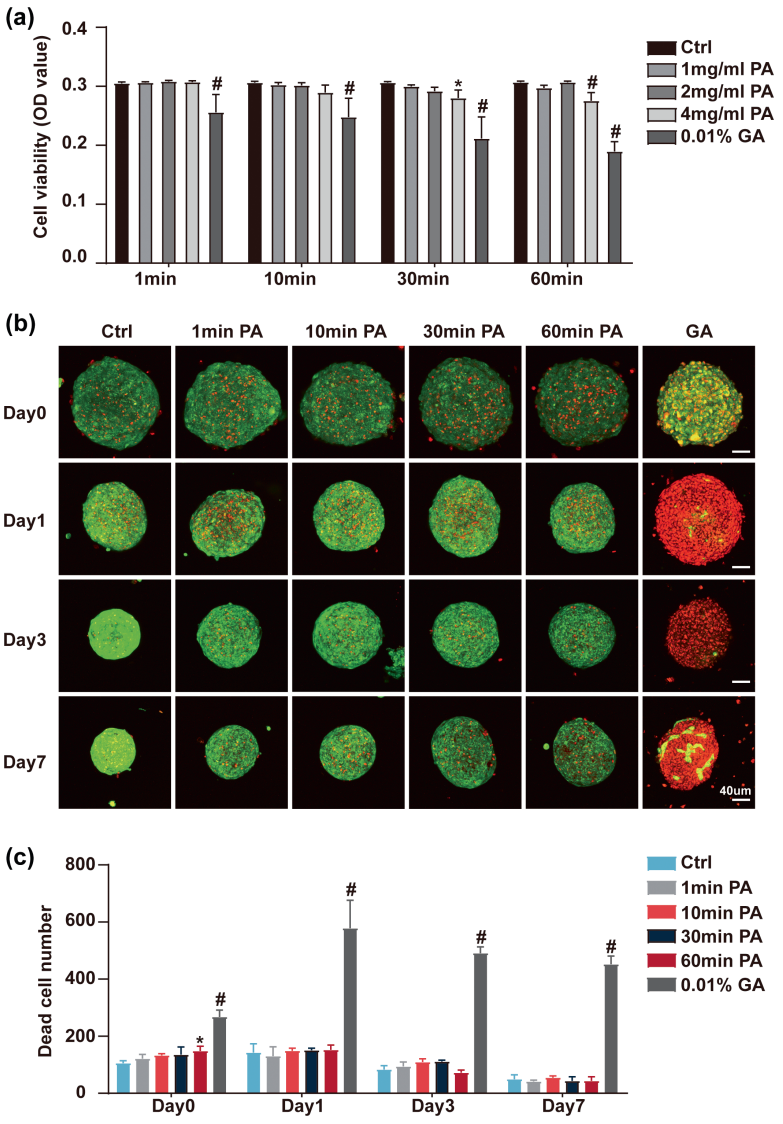

FIGURE 3 Effects of PA preconditioning on cell viability of microtissue spheroids. (a) MTT assay tested the effect of PA treatment (1, 2, 4 mg/mL) for 1, 10, 30, and 60 min on cell viability of DPSCs. (b) Fluorescence images and (c) dead cell number of live/dead staining after 1 mg/mL PA preconditioning for 1, 10, 30, and 60 min in microtissues after 0, 1, 3, and 7 days. 0.01% GA-preconditioning for 1 min was used as a positive control. Compared with the control group, $^{*}p < 0.05$, $^{\#}p < 0.0001$.

decreased cell viability; hence, 1 mg/mL was chosen as the concentration for testing its effects on cell viability of microtissue spheroids.

In Figure 3b, c, live/dead assay showed that 0.01% GA treatment for 1 min caused a significantly higher number of dead cells within microtissue spheroids in the following 1, 3, and 7 days ($p < 0.0001$). In contrast, there were no significant changes in dead cell number between 1 mg/mL PA treatment for 1 min, 10 min, 30 min, and the control group ($p > 0.05$) in all tested time points. A slightly higher number of dead cells was observed on day 0 for the group that received 1 mg/mL PA treatment for 60 min ($p < 0.05$), but no significant changes in cell viability were examined in the following 1, 3, and 7 days. Collectively, 1 mg/mL PA treatment for 1, 10, 30, and 60 min has good biocompatibility and causes no adverse effects on the cell viability of DPSC microtissue spheroids; therefore, this condition was utilized for subsequent tests.

Effects of PA treatment on structural and dimensional stability of microtissue and macrotissue spheroids and the role of F-Actin

Surface stiffness of microtissue spheroids was measured to assess the effect of PA treatment (1 mg/mL PA for 30 and 60 min) on their mechanical strength (Figure 4a). Compared with the control group, an increased surface stiffness was tested after 30 min PA treatment ($p < 0.01$).

The transverse area of microtissue spheroids was measured for up to 7 days to assess the effects of PA treatment (1 mg/mL PA for 60 min) on their dimensional stability (Figure 4d–f). In the control group, the microtissue dimension decreased since day1 and dropped until day7 (under basal and OS culture). In contrast, spheroid dimension increased before day3 under OS induction and before day1 under basal culture in the PA-treated group. A significantly less dimensional shrinkage was observed in

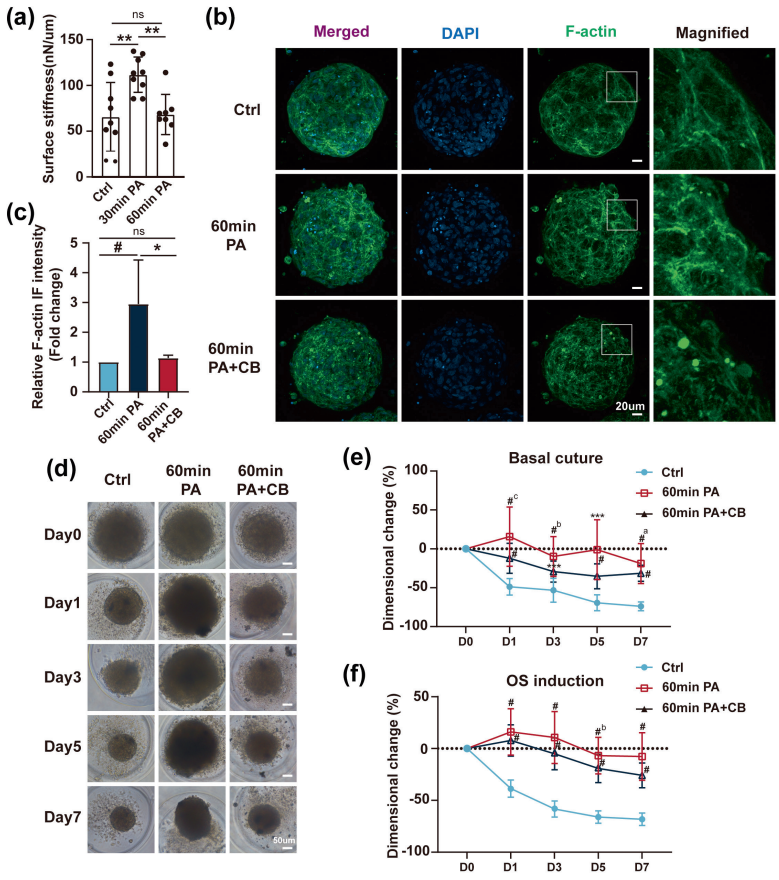

FIGURE 4 PA preconditioning regulates cytoskeletal F-Actin to maintain dimensional stability. (a) Surface stiffness of control, 30 and 60 min PA-preconditioned (1 mg/mL) microtissues by Bio-AFM analysis. (b) Observation of cytoskeletal F-Actin distribution and (c) their relative IF expression level in control, 60 min PA or 60 min PA + CB-treated microtissues. (d) Representative images of control, 60 min PA, 60 min PA + CB-treated microtissues under basal culture condition over 7 days. Quantification of dimensional changes of control, 60 min PA or 60 min PA + CB microtissues-treated under basal (e) or OS induction culture (f). Compared with the control group, $*p < 0.05$, $**p < 0.01$, $***p < 0.01$, $^{\#}p < 0.0001$. Compared with the 60 min PA + CB group, $^{a}p < 0.05$, $^{b}p < 0.01$, $^{c}p < 0.001$.

all tested time points (Figure 4e, f, $p < 0.001$) after PA treatment under basal and OS culture, indicating a positive role of PA treatment in preventing microtissue shrinkage.

To explore the effects of PA treatment on F-actin activity within microtissues, F-actin distribution was visualized through IF staining (Figure 4b). Compared with the control group, PA treatment induced a significantly higher F-actin expression (Figure 4c, $p < 0.0001$). Next, to study the regulatory role of F-actin after PA treatment, a cell-permeable mycotoxin cytochalasin B (CB) was added together with PA to disrupt the polymerization of cytoskeletal actin (Figure 4b, c). Compared with PA group, inhibition of F-actin activity (in PA + CB group) resulted in more dimensional shrinkage at day1 ($p < 0.001$), day3 ($p < 0.01$) and day7 ($p < 0.05$) (Figure 4d, e, under basal culture). Under OS culture, an increased dimensional shrinkage was also observed in PA + CB group at day5 (Figure 4f, $p < 0.01$), indicating a regulatory role of F-actin in PA-induced dimensional stability in microtissue spheroids.

To test the effects of PA preconditioning on the assembly of microtissues into a macrotissue, microtissues from one 3D Petri dish (~768 microtissues) were collected, allowed to self-assemble for 4 days (Figure 2c, d), single-cycle PA treatment was introduced, and then cultured for 7 or 14 days. H&E staining of PA-treated macrotissues was performed as shown in Figure 5a, which displayed histological structures of macrotissues. Quantification of macrotissue dimension in Figure 5b, c indicated that 30- and 60-min PA treatment induced a larger transverse-section area after 7 days in vitro culture, with a significantly larger area in the 30-min PA group ($p < 0.01$). Similarly, after culturing for 14 days, a larger area was observed in the 30-min PA group ($p < 0.01$). These results indicated an effective role of PA treatment in maintaining both microtissue and macrotissue structure size.

Masson trichrome staining was conducted to observe collagen formation within macrotissues in Figure 6a, b. Quantifying the collagen area in Figure 6c, d implied that 30-min PA treatment induced more collagen formed within macrotissues under 7-day basal and 14-day OS conditions.

Effects of PA treatment on biomineralization of microtissue and microtissue spheroids

Alizarin red staining in Figure 7a, b showed mineralized nodule formation of 30- and 60-min PA-treated macrotissues cultured for 7 and 14 days. Quantifying mineralized nodule number showed that significantly more mineralized nodules were formed within 60-min PA-treated

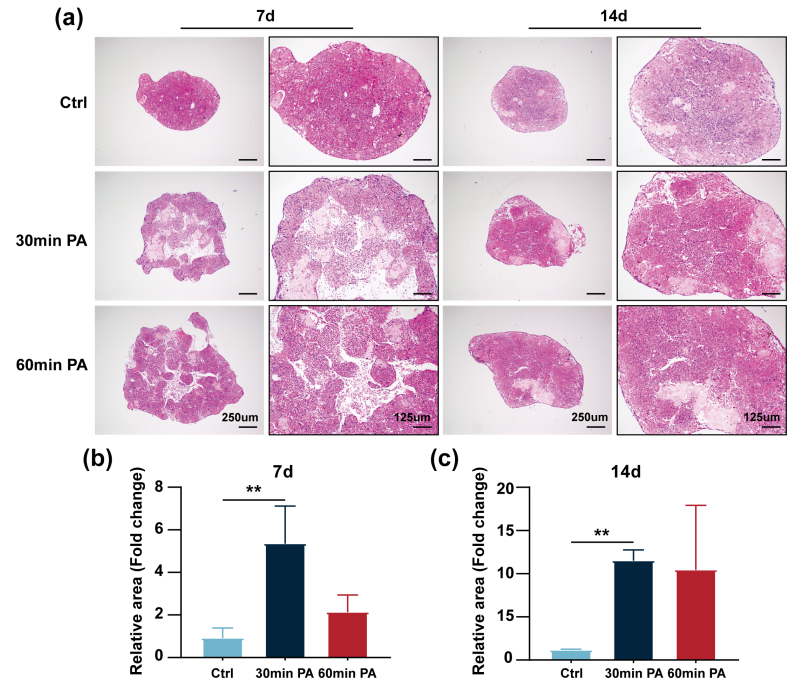

FIGURE 5 Histological analysis of PA-preconditioned macrotissue spheroids. Histological analysis of 30 and 60 min PA-preconditioned (1 mg/mL) macrotissues by HE staining (a). Macrotissue spheroids were cultured under basal conditions for 7 days and 14 days. Quantification of the relative area of macrotissue spheroids after culturing 7 days (b) and 14 days (c). Compared with the control group, $^{**}p < 0.01$.

macrotissues in basal and OS conditions at days 7 and 14 ($p < 0.05$). Similarly, a larger mineralized area was also detected in 60-min PA-treated macrotissues under OS condition (at day 7 and day 14; $p < 0.05$) and basal condition (at day 14; $p < 0.05$).

IHC staining of ALP in Figure 8a, b showed ALP protein expression in 30- and 60-min PA-treated macrotissues cultured under basal and OS induction conditions for 7 and 14 days. Quantification of ALP expression indicated that 30- and 60-min PA treatment induced a higher proportion of ALP-expressing area in PA-treated macrotissues ($p < 0.05$). Odontoblastic differentiation marker DMP-1 was also checked by IHC staining in Figure 9a, b, with a higher proportion of DMP-1-positive area in 60-min PA-treated macrotissues under OS induction for 14 days ($p < 0.001$). Besides, ALP activity was also assessed in PA-treated microtissues; Figure 8e showed that 30-min PA treatment induced significantly higher ALP activity than the control group under basal conditions ($p < 0.0001$). Intriguingly, 60-min PA treatment induced concurrently higher DSPP and F-actin expression in microtissues (OS induction for 7 days, Figure 10a–c). When F-actin activity was inhibited by CB, a significantly lower expression of DSPP and F-actin was revealed (in PA + CB group), indicating the important role of cytoskeletal F-actin during PA-induced biomineralization in microtissue spheroids.

DISCUSSION

Cell spheroids emerge as a biocompatible scaffold-free method for delivering cells within a host environment, offering application potentials for pulp regeneration. The inherent self-assembly capability of cell spheroids contributes to their enhanced viability and adaptability; however, their mechanical resilience is comparatively modest, rendering them susceptible to damage during manipulation and progressive volumetric reduction over time. To address this, reinforcing surface protection of tissue spheroids appears as a prospective means of maintaining tissue structure and viability. Derived from plants and serving as a natural collagen cross-linker, PA has demonstrated the ability to enhance cell proliferation and facilitate osteoblast differentiation following pretreatment within scaffolds. Herein, our study, for the first time, introduced the concept of surface preconditioning using a collagen cross-linking agent, PA, which can potentially create a cross-linked layer of collagen fibres derived from extracellular matrix (ECM) on the spheroid surface. This newly formed layer operates as a discrete micro-scaffold, subtly integrated within the spheroidal structure, enhancing tissue stability and promoting biomineralization.

To examine the biocompatibility of PA precondition as a strategy, we first assessed PA's effects on the cell viability of DPSC microtissue spheroids. As our aim was surface preconditioning, we only introduced a single treatment cycle as a preconditioning method and used 1–4 mg/mL PA solution in time durations from 1 min to 1 h. We found that 1–2 mg/mL PA concentrations had no significant adverse effect on the cell viability of DPSCs. This finding is consistent with a previous report that different concentrations of grape seed extract (0.0065%–6.5%), which contains 95% PA, treated for 1–60 min had no significant toxic effect on dental pulp cells (dos Santos et al., 2019). In addition,

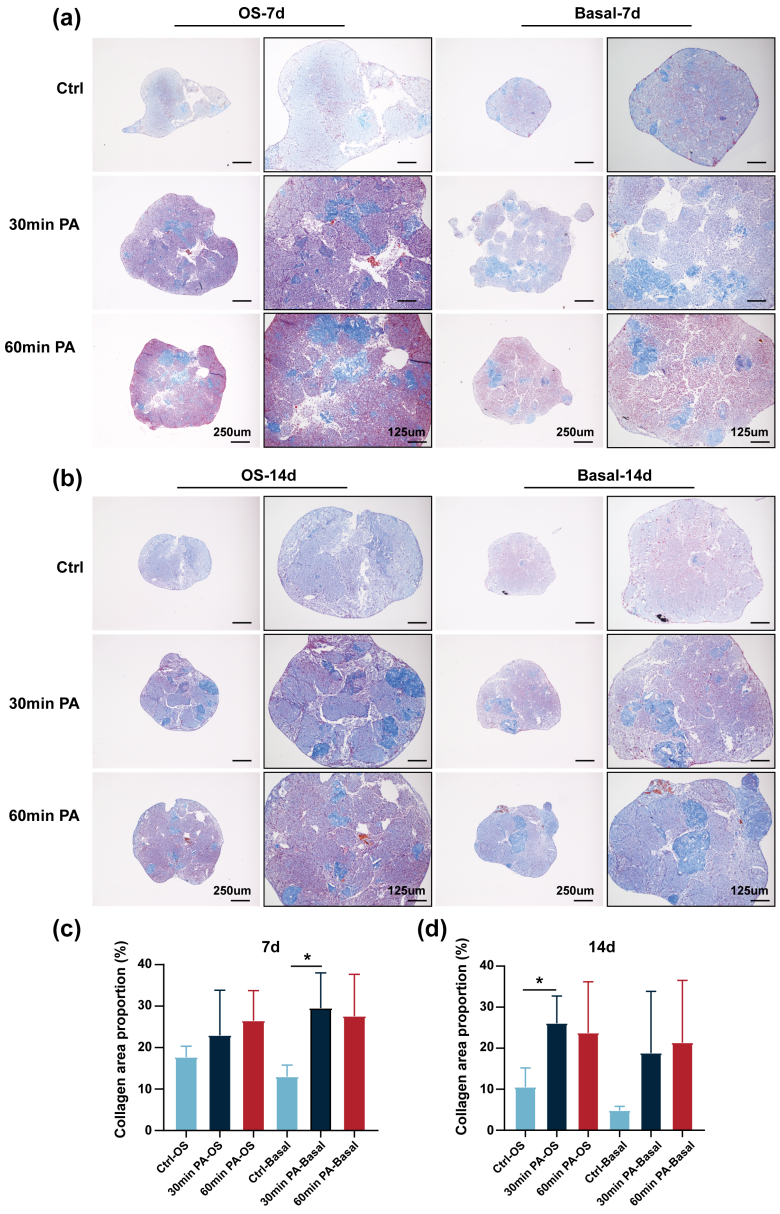

FIGURE 6 Collagen formation in PA-preconditioned macrotissue spheroids. Collagen formation analysis of 30 and 60 min PA-preconditioned (1 mg/mL) macrotissues by Masson Trichrome staining. Macrotissue spheroids were cultured under OS induction and basal conditions for 7 days (a) and 14 days (b). Quantification of the proportion of collagen area within macrotissue spheroids after culturing 7 days (c) and 14 days (d). Compared with the control group, $*p < 0.05$.

we have postulated that grape seed extract may have a biostimulating role and protect dental pulp cells (dos Santos et al., 2019). When evaluating cellular metabolism using the MTT assay, we could see nearly a 10% reduction in the 30- and 60-min treatment of 4 mg/mL PA; therefore, 1 mg/mL was considered the safest concentration in our study. Similarly, in a previous study, this selected concentration has shown increased cell proliferation of gingival fibroblast cells (Kurauchi et al., 2014). Moreover, the residual toxic effects of PA treatment on microtissue were examined by assessing dead cell numbers from day 1 to 7. As shown in Figure 3, up to 1 h of treatment of 1 mg/mL PA did not demonstrate significant cell death over 7 days. Although some increase in dead cell number was observed immediately after PA treatment, the cells tended to recover when returned to standard medium, and the spheroids reached a balance between cell death and proliferation.

Despite stabilizing the spheroid surface, minimizing its influence on cellular metabolism within inner spheroids is essential. Given that our intervention is primarily directed towards the surface cell layer and the extracellular matrix (ECM), the impact of PA preconditioning on spheroid cellular metabolism should be negligible. Microtissue spheroids consist of distinct cellular layers, typically characterized by a highly proliferative outer layer, while innermost cells tend to be senescent or necrotic. The outer layer's robust proliferation can be attributed to its readily available oxygen and nutrient supply. Conversely, without adequate oxygen or nutrients, central core cells may undergo necrosis (Costa et al., 2016). It is speculated that oxygen and other biomolecules diffuse across a few hundred microns within spheroids (Shen et al., 2021); in our study, the microtissues were in a range of 200 μm, and we did not observe many necrotic foci inside the tissues, nor

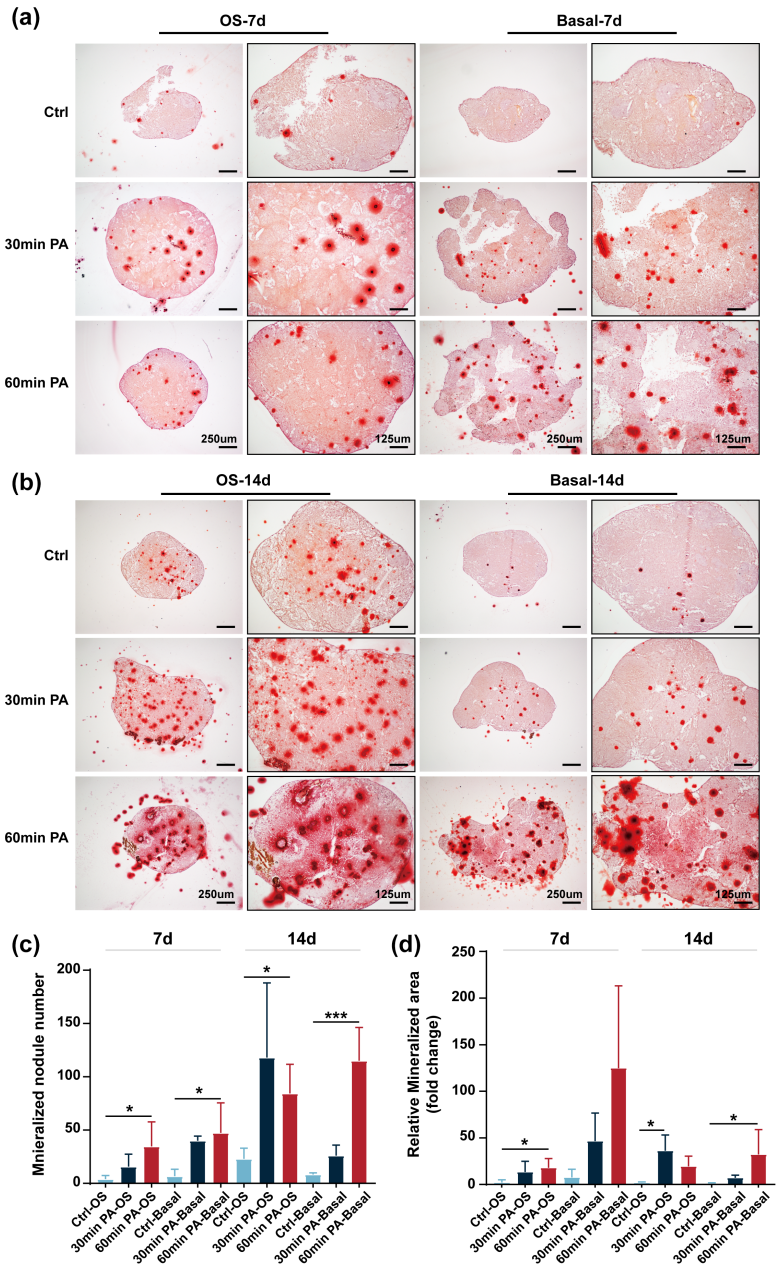

FIGURE 7 Biomineralization of PA-preconditioned macrotissue spheroids. Biomineralization analysis of 30 and 60 min PA-preconditioned (1 mg/mL) macrotissues by Alizarin red staining. Macrotissue spheroids were cultured under OS induction and basal conditions for 7 days (a) and 14 days (b). Quantification of mineralized nodules number (c) and relative mineralized area (d) of macrotissue spheroids after culturing 7 and 14 days. Compared with the control group, $*p < 0.05$, $***p < 0.001$.

noticeable surface cell death was revealed by the live/dead cell imaging. Additionally, when observed in H&E sections, no significant amounts of necrotic foci were present inside the PA-treated macrotissues. From these findings, we determined that the PA preconditioning of microtissue and macrotissue surfaces is unlikely to affect their cellular mechanisms significantly.

Several studies reported that over-time shrinkage or temporal decreased volume of cell spheroid hinders its application for tissue engineering (Bellotti et al., 2016; Deynoux et al., 2020; Redondo-Castro et al., 2018; Schmal et al., 2016; Shearier et al., 2016). This finding is consistent with our observation that a significant shrinkage occurred over 7 days. As a novel remedy, our study supported that PA-preconditioning effectively reduced the tissue volume shrinkage. Under both basal and OS induction culture, microtissue treated for 60 min with PA showed less dimensional shrinkage compared to the control group. It was reported that actin-associated cytoskeleton change is critical for 3D spheroid fabrication and their biological functions (Kai et al., 2022; Lee et al., 2020; Weidemann et al., 2013), and our results regarding surface stiffness changes after PA treatment also implies the alteration of cytoskeleton and mechanotransduction in spheroids. Therefore, we further tested the F-actin activity after PA-preconditioning and found it induced a higher F-actin expression along with F-actin distribution re-organization on spheroid surface. More importantly, inhibition of F-actin polymerization by cytochalasin B dismissed PA's role in dimensional stability, implying that PA's role in dimensional stability

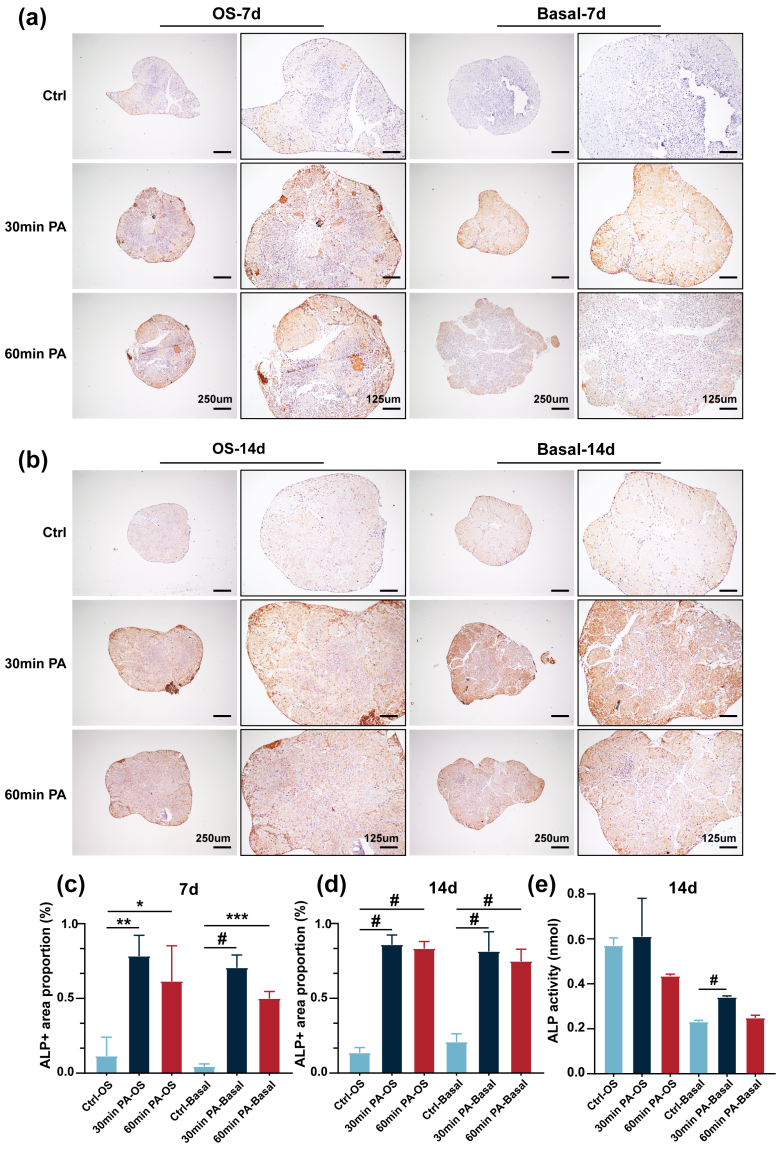

FIGURE 8 ALP activity in PA-preconditioned macrotissue and microtissue spheroids. (a–d) ALP expression in 30 and 60 min PA-preconditioned (1 mg/mL) macrotissues by IHC staining. Macrotissue spheroids were cultured under OS induction and basal conditions for 7 days (a) and 14 days (b). Quantifying ALP-positive area proportion in macrotissue spheroids after culturing for 7 days (c) and 14 days (d). (e) ALP activity (protein level) of PA-preconditioned (1 mg/mL) microtissues tested by ALP test kit. Compared with control group, $^{*}p < 0.05$, $^{**}p < 0.01$, $^{***}p < 0.001$, $^{\#}p < 0.0001$.

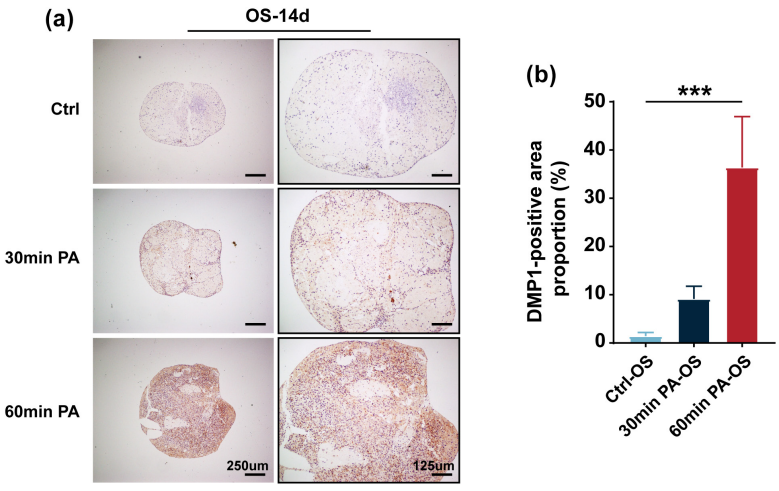

FIGURE 9 DMP-1 expression in PA-preconditioned macrotissue spheroids by IHC staining. DMP-1 expression in 30 and 60-min PA-preconditioned (1 mg/mL) macrotissues by IHC staining. (a) Macrotissue spheroids were cultured under OS induction and basal conditions for 14 days. (b) Quantification of DMP1-positive area proportion in macrotissue spheroids after culturing for 14 days. Compared with the control group, $^{***}p < 0.001$.

may be partially through its regulation on actin-associated cytoskeleton change.

Previous work indicates that volume shrinkage may result from the imbalance between cell death and proliferation over time (Deynoux et al., 2020), hence, PA's regulation on cell proliferation may also involve the shrinkage of spheroids. Firstly, PA is known to induce cell proliferation and can enhance the cell proliferation rate

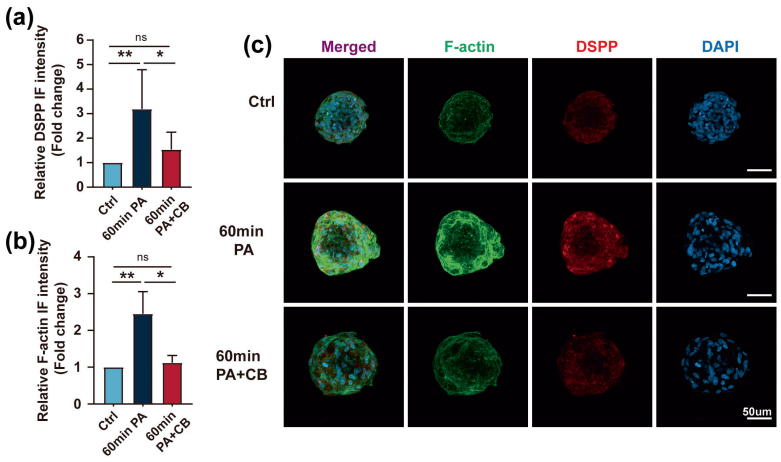

FIGURE 10 PA preconditioning regulates cytoskeletal F-Actin to upregulate DSPP expression in microtissue spheroids. DSPP (a) and F-Actin (b) expression level of control, 60 min PA, 60 min PA + CB-treated microtissues after OS induction for 7 days. (c) Representative images of DSPP and F-Actin expression through IF staining of microtissues. $*p < 0.05$, $**p < 0.01$.

of the outmost cell later. Scaffold surfaces treated with PA show higher cell proliferation and migration. We can consider that PA-treated surface cells and ECM layer could act as a micro-scaffold. For instance, PA-treated gelatin/chitosan scaffolds were non-cytotoxic to fibroblasts and promoted the attachment and proliferation of the seeded cells (Yang et al., 2017). Additionally, collagen films cross-linked with PA demonstrated faster cell proliferation of human osteoblast cells (Yang et al., 2021). Secondly, PA can induce collagen formation in ECM, which could lead to the microtissue spheroid's stability. It was shown that anthocyanins stimulated the expression of ECM proteins, such as collagen (types I and III) and elastin in skin fibroblasts (Nanashima et al., 2018). PA is a well-defined natural cross-linking reagent for stabilizing collagen matrices (Han et al., 2003); hence, when cell spheroids were pretreated with PA, the spheroids surface ECM could become cross-linked and act like a biofunctional surface. The cross-linked ECM between cells would allow a micro-scaffold for cells to continue cell proliferation. Overall, the size reduction does not seem to be strictly attributable to reduced cell number in spheroids and could be possibly attributed to other factors such as the ECM composition (Deynoux et al., 2020).

Furthermore, we also used PA to precondition fusing microtissues to test its effects on maintaining larger-size macrotissues. During the early-stage fusion of multiple microtissues, the PA treatment was introduced. As shown in HE images, 30-min PA-preconditioning induced a significantly larger tissue area of fused macrotissues; this can be attributed to two possible aspects triggered by PA precondition. Firstly, the volume increase is related to the tissue stabilization induced by cross-linking outside the macrotissue surface. Compared with no treatment, lower cell density and more sparse tissue structure were observed in the core of PA-preconditioned macrotissues. It has been estimated that the cross-linked surface generated a more stable periphery structure, entailing more inner space for microtissue distribution and growth. This effect can be especially beneficial to cell survival of the larger-size tissue, as more oxygen and nutrients will penetrate the inner macrotissue, alleviating the hypoxic microenvironment. Secondly, the increased area may result from more collagen formation within the macrotissue, as observed in Masson trichrome staining, especially since those collagen bulks are filled in microtissue gaps. Nevertheless, further verification is required to determine whether the secreted collagen is from the biomineralization triggered by PA or the collagen network cross-linking within the macrotissue.

The additional advantage of PA in tissue regeneration is its promotional role in biomineralization. It was shown that PA has an osteogenic effect on dental pulp cells when embedded within PA-treated dentine. The exposure to PA increased the expression of crucial biomineralization and odontogenic differentiation regulators, including RUNX2, BMP2, OCN, and DSPP (Kulakowski et al., 2017). Moreover, when mesenchymal stem cells were treated with polyphenols extracted from grape pomace, cells exhibited differentiation to osteoblasts and mineralization (Torre et al., 2020). In a simplified dentin-dental pulp cell (DPC) complex model, DPCs embedded within their native ECM in the presence of PAC-treated dentin exhibited increased proliferation. Overall, the results suggested that PAC dimers, trimers, and tetramers are biocompatible and enhance the differentiation of DPCs towards a phenotype that favours biomineralization. PAC-enriched refined compositions can influence the field of biomaterials and regeneration by serving as renewable, non-cytotoxic agents that can increase the mechanical properties of biomaterials (Kulakowski et al., 2017). In our study, PA treatment could not stimulate significant ALP activity in microtissue only when induced with an osteogenic induction medium; the ALP production increased in the group where 1 mg/mL PA was used for 30 min under basal conditions. However, for macrotissues, 30- or 60 min of

PA treatment increased ALP expression. Besides, 60 min of PA treatment triggered higher expression of DMP-1 in OS-induced macrotissues. Combined, mineralized nodule formation in 60-min PA-treated groups displayed a more robust effect on promoting biomineralization. Additionally, our result that concurrently higher DSPP and F-actin expression in microtissue after PA treatment and inhibition of F-actin activity significantly attenuated the upregulation, indicating the critical role of cytoskeletal F-actin during PA-induced odontoblastic differentiation and biomineralization in microtissue spheroids.

Recent evidence indicates that stem cell spheroids have been applied for advanced therapeutic purposes in tissue regeneration and repair (Dissanayaka & Zhang, 2020; Kim et al., 2023). Our previous work have demonstrated that the scaffold-free prevascularized microtissue spheroids can successfully regenerate vascular dental pulp-like tissue in vivo (Dissanayaka et al., 2014). Given that PA is already widely used in dentin adhesion, it can be especially suitable for application in the dental pulp chamber; its multi-faceted role in enhancing dentin adhesion, tissue stability, and biomineralization offers new methods for in situ pulp regeneration.

CONCLUSION

In conclusion, this study presents a novel strategy for enhancing scaffold-free cell spheroids' structural integrity and biomineralization potential. The natural collagen cross-linker, PA, demonstrated remarkable biocompatibility as a surface preconditioning agent that could effectively enhance dimensional stability and biomineralization of DPSC microtissue spheroids, which is promising for in situ pulp regeneration.

AUTHOR CONTRIBUTIONS

Shengyan Yang: Data acquisition, Data analysis, Visualization, Writing—original draft. Andy Yu Pan Leung & Zheng Wang: Data acquisition. Cynthia Kar Yung Yiu: Writing—review & editing. Waruna Lakmal Dissanayaka: Conceptualization, Supervision, Project administration, Funding acquisition, Writing—review & editing.

ACKNOWLEDGEMENTS

We thank Mr. Geoffrey Ng for the excellent technical support during our experiments.

FUNDING INFORMATION

This research was supported by the Research Grants Council, Hong Kong (General Research Fund; 17125421) and The University of Hong Kong (Seed Fund for PI Research—Basic Research; 104006640).

CONFLICT OF INTEREST STATEMENT

We declare that there was no conflict of interest in this study.

DATA AVAILABILITY STATEMENT

Data will be made available on request.

ETHICS STATEMENT

All biological procedures described were performed according to the regulations and guidelines of the University of Hong Kong.

ORCID

Waruna Lakmal Dissanayaka https://orcid.org/0000-0002-3621-4866

REFERENCES

Adamiak, K. & Sionkowska, A. (2020) Current methods of collagen cross-linking: review. *International Journal of Biological Macromolecules*, 161, 550–560.

Bellotti, C., Duchi, S., Bevilacqua, A., Lucarelli, E. & Piccinini, F. (2016) Long term morphological characterization of mesenchymal stromal cells 3D spheroids built with a rapid method based on entry-level equipment. *Cytotechnology*, 68, 2479–2490.

Calori, I.R., Alves, S.R., Bi, H. & Tedesco, A.C. (2022) Type-I collagen/collagenase modulates the 3D structure and behavior of glioblastoma spheroid models. *ACS Applied Bio Materials*, 5, 723–733.

Chen, H., Wang, W.Y., Yu, S.Y., Wang, H.M., Tian, Z.L. & Zhu, S. (2022) Procyanidins and their therapeutic potential against oral diseases. *Molecules*, 27, 2932.

Costa, E.C., Moreira, A.F., De Melo-Diogo, D., Gaspar, V.M., Carvalho, M.P. & Correia, I.J. (2016) 3D tumor spheroids: an overview on the tools and techniques used for their analysis. *Biotechnology Advances*, 34, 1427–1441.

Deynoux, M., Sunter, N., Ducrocq, E., Dakik, H., Guibon, R., Burlaud-Gaillard, J. et al. (2020) A comparative study of the capacity of mesenchymal stromal cell lines to form spheroids. *PLoS One*, 15, e0225485.

Dissanayaka, W.L. & Zhang, C.F. (2020) Scaffold-based and scaffold-free strategies in dental pulp regeneration. *Journal of Endodontics*, 46, S81–S89.

Dissanayaka, W.L., Zhu, L., Hargreaves, K.M., Jin, L. & Zhang, C. (2014) Scaffold-free Prevascularized microtissue spheroids for pulp regeneration. *Journal of Dental Research*, 93, 1296–1303.

Dissanayaka, W.L., Zhu, L.F., Hargreaves, K.M., Fin, L.J. & Zhang, C.F. (2015) In vitro analysis of scaffold-free Prevascularized microtissue spheroids containing human dental pulp cells and endothelial cells. *Journal of Endodontics*, 41, 663–670.

Dos Santos, A.F., Pacheco, J.M., Silva, P.A.O., Bedran-Russo, A.K., Rezende, T.M.B., Pereira, P.N.R. et al. (2019) Direct and transdentinal biostimulatory effects of grape seed extract rich in

proanthocyanidin on pulp cells. *International Endodontic Journal*, 52, 424–438.

Gonzalez-Fernandez, T., Tenorio, A.J., Saiz, A.M. & Leach, J.K. (2022) Engineered cell-secreted extracellular matrix modulates cell spheroid Mechanosensing and amplifies their response to inductive cues for the formation of mineralized tissues. *Advanced Healthcare Materials*, 11, e2102337.

Gu, L.S., Shan, T.T., Ma, Y.X., Tay, F.R. & Niu, L.N. (2019) Novel biomedical applications of Crosslinked collagen. *Trends in Biotechnology*, 37, 464–491.

Han, B., Jaurequi, J., Tang, B.W. & Nimni, M.E. (2003) Proanthocyanidin: a natural crosslinking reagent for stabilizing collagen matrices. *Journal of Biomedical Materials Research Part A*, 65A, 118–124.

He, J., Zhang, N.H., Zhu, Y., Jin, R.R. & Wu, F. (2021) MSC spheroids-loaded collagen hydrogels simultaneously promote neuronal differentiation and suppress inflammatory reaction through PI3K-Akt signaling pathway. *Biomaterials*, 265, 120448.

Kageyama, T., Akieda, H., Sonoyama, Y., Sato, K., Yoshikawa, H., Isono, H. et al. (2023) Bone beads enveloped with vascular endothelial cells for bone regenerative medicine*. *Acta Biomaterialia*, 165, 168–179.

Kai, F., Ou, G.Q., Tourdot, R.W., Stashko, C., Gaietta, G., Swift, M.F. et al. (2022) ECM dimensionality tunes Actin tension to modulate endoplasmic reticulum function and spheroid phenotypes of mammary epithelial cells. *EMBO Journal*, 41, e109205.

Kelm, J.M., Djonov, V., Ittner, L.M., Fluri, D., Born, W., Hoerstrup, S.P. et al. (2006) Design of custom-shaped vascularized tissues using microtissue spheroids as minimal building units. *Tissue Engineering*, 12, 2151–2160.

Kelm, J.M. & Fussenegger, M. (2004) Microscale tissue engineering using gravity-enforced cell assembly. *Trends in Biotechnology*, 22, 195–202.

Kim, H., Choi, N., Kim, D.Y., Kim, S.Y., Song, S.Y. & Sung, J.H. (2021) TGF-β2 and collagen play pivotal roles in the spheroid formation and anti-aging of human dermal papilla cells. *Aging*, 13, 19978–19995.

Kim, W., Gwon, Y., Park, S., Kim, H. & Kim, J. (2023) Therapeutic strategies of three-dimensional stem cell spheroids and organoids for tissue repair and regeneration. *Bioactive Materials*, 19, 50–74.

Kulakowski, D., Leme-Kraus, A.A., Nama, J.W., Mcalpine, J., Chen, S.N., Pauli, G.F. et al. (2017) Oligomeric proanthocyanidins released from dentin induce regenerative dental pulp cell response. *Acta Biomaterialia*, 55, 262–270.

Kurauchi, M., Niwano, Y., Shirato, M., Kanno, T., Nakamura, K., Egusa, H. et al. (2014) Cytoprotective effect of short-term pretreatment with Proanthocyanidin on human gingival fibroblasts exposed to harsh environmental conditions. *PLoS One*, 9, e113403.

Lee, C.F., Hsu, Y.H., Lin, Y.C., Nguyen, T.T., Chen, H.W., Nabilla, S.C. et al. (2021) 3D printing of collagen/Oligomeric Proanthocyanidin/oxidized hyaluronic acid composite scaffolds for articular cartilage repair. *Polymers*, 13, 3123.

Lee, Y.N., Yi, H.J., Goh, H., Park, J.Y., Ferber, S., Shim, I.K. et al. (2020) Spheroid fabrication using concave microwells enhances the differentiation efficacy and function of insulin-producing cells via cytoskeletal changes. *Cells*, 9, 2551.

Li, L.L., Liu, X.F., Gaihre, B., Li, Y. & Lu, L.C. (2021) Mesenchymal stem cell spheroids incorporated with collagen and black phosphorus promote osteogenesis of biodegradable hydrogels. *Materials Science & Engineering, C: Materials for Biological Applications*, 121, 111812.

Nanashima, N., Horie, K., Maeda, H., Tomisawa, T., Kitajima, M. & Nakamura, T. (2018) Blackcurrant Anthocyanins increase the levels of collagen, elastin, and hyaluronic acid in human skin fibroblasts and Ovariectomized rats. *Nutrients*, 10, 495.

Ovsianikov, A., Khademhosseini, A. & Mironov, V. (2018) The synergy of scaffold-based and scaffold-free tissue engineering strategies. *Trends in Biotechnology*, 36, 348–357.

Rauf, A., Imran, M., Abu-Izneid, T., Iahfisham Ul, H., Patel, S., Pan, X.D. et al. (2019) Proanthocyanidins: a comprehensive review. *Biomedicine & Pharmacotherapy*, 116, 108999.

Redondo-Castro, E., Cunningham, C.J., Miller, J., Cain, S.A., Allan, S.M. & Pinteaux, E. (2018) Generation of human mesenchymal stem cell 3D spheroids using low-binding plates. *Bio-Protocol*, 8, e2968.

Schmal, O., Seifert, J., Schaffer, T.E., Walter, C.B., Aicher, W.K. & Klein, G. (2016) Hematopoietic stem and progenitor cell expansion in contact with mesenchymal stromal cells in a hanging drop model uncovers disadvantages of 3D culture. *Stem Cells International*, 2016, 4148093.

Shajib, M.S., Futrega, K., Klein, T.J., Crawford, R.W. & Doran, M.R. (2022) Collagenase treatment appears to improve cartilage tissue integration but damage to collagen networks is likely permanent. *Journal of Tissue Engineering*, 13, 1–19.

Shearier, E., Xing, Q., Qian, Z.C. & Zhao, F. (2016) Physiologically low oxygen enhances biomolecule production and Stemness of mesenchymal stem cell spheroids. *Tissue Engineering Part C-Methods*, 22, 360–369.

Shen, H.L., Cai, S.X., Wu, C.X., Yang, W.G., Yu, H.B. & Liu, L.Q. (2021) Recent advances in three-dimensional multicellular spheroid culture and future development. *Micromachines*, 12, 96.

Sorushanova, A., Delgado, L.M., Wu, Z.N., Shologu, N., Kshirsagar, A., Raghunath, R. et al. (2019) The collagen Suprafamily: from biosynthesis to advanced biomaterial development. *Advanced Materials*, 31, e1801651.

Torre, E., Iviglia, G., Cassinelli, C., Morra, M. & Russo, N. (2020) Polyphenols from grape pomace induce osteogenic differentiation in mesenchymal stem cells. *International Journal of Molecular Medicine*, 45, 1721–1734.

Walters, B.D. & Stegemann, J.P. (2014) Strategies for directing the structure and function of three-dimensional collagen biomaterials across length scales. *Acta Biomaterialia*, 10, 1488–1501.

Weidemann, A., Breyer, J., Rehm, M., Eckardt, K.U., Daniel, C., Cicha, I. et al. (2013) HIF-1α activation results in Actin cytoskeleton reorganization and modulation of Rac-1 signaling in endothelial cells. *Cell Communication and Signaling*, 11, 80.

Yang, H.F., Liu, W.C., Liu, X.R., Li, Y.Q., Lin, C.P., Lin, Y.M. et al. (2021) Study on proanthocyanidins crosslinked collagen membrane for guided bone tissue regeneration. *Journal of Applied Biomaterials & Functional Materials*, 19, 228080002110053.

Yang, Y., Ritchie, A.C. & Everitt, N.M. (2017) Comparison of glutaraldehyde and procyanidin cross-linked scaffolds for soft tissue engineering. *Materials Science & Engineering, C: Materials for Biological Applications*, 80, 263–273.

Zhang, Y.C., Liu, J.Q., Zou, T., Qi, Y.B.Q., Yi, B.C., Dissanayaka, W.L. et al. (2021) DPSCs treated by TGF-β1 regulate angiogenic sprouting of three-dimensionally co-cultured HUVECs and DPSCs through VEGF-Ang-Tie2 signaling. *Stem Cell Research & Therapy*, 12, 281.

Zheng, M.H., Wang, X.C., Chen, Y.N., Yue, O.Y., Bai, Z.X., Cui, B.Q. et al. (2023) A review of recent progress on collagen-based biomaterials. *Advanced Healthcare Materials*, 12, e2202042.

How to cite this article: Yang, S., Leung, A.Y.P., Wang, Z., Yiu, C.K.Y. & Dissanayaka, W.L. (2024) Proanthocyanidin surface preconditioning of dental pulp stem cell spheroids enhances dimensional stability and biomineralization in vitro. *International Endodontic Journal*, 00, 1–16. Available from: https://doi.org/10.1111/iej.14126